Neutron $3s_{1/2}$ occupation change across the stable tin isotopes investigated using isotopic analysis of proton scattering at 295 MeV

Yoshiko Kanada-En'yo
Department of Physics, Kyoto University, Kyoto 606-8502, Japan

(Received 3 August 2022; accepted 14 September 2022; published 27 September 2022)

The isotopic systematics of Sn isotopes in the range $A = 116$–124 were investigated by combining the nuclear structure and reaction calculations for the analysis of ^{A}Sn(p, p) reactions at 295 MeV. The ^{A}Sn(p, p) reactions were calculated employing the relativistic impulse approximation (RIA) with theoretical densities obtained for the Sn isotopes from relativistic Hartree-Bogoliubov (RHB) calculations with the DD-ME2 interaction and nonrelativistic Skyrme Hartree-Fock-Bogoliubov (SHFB) calculations with the SKM* interaction. Calculation using the DD-ME2 density reproduced the experimental data for ^{122}Sn(p, p) but overestimated the ^{116}Sn(p, p) and ^{118}Sn(p, p) cross sections at backward angles. In the isotopic analysis of the cross section ratio $R(\sigma)$ of ^{122}Sn to ^{116}Sn, a calculation using the SKM* density reproduced the peak amplitudes of $R(\sigma)$ obtained from the experimental cross sections, whereas a calculation using the DD-ME2 density did not. The ratio $R(\sigma)$ was found to be sensitive to the isotopic change of the neutron $3s_{1/2}$ occupation through the isotopic difference of the surface neutron density around $r = 4$–5 fm. Isotopic analysis indicated that a rapid increase of the $3s_{1/2}$ occupation from ^{116}Sn to ^{122}Sn obtained by the DD-ME2 calculation is unlikely. This result derived from the 295 MeV ^{A}Sn(p, p) cross section data [S. Terashima *et al.*, Phys. Rev. C **77**, 024317 (2008).] is consistent with the direct measurement of the neutron occupations in Sn isotopes by neutron transfer and pickup reactions [S. V. Szwec *et al.*, Phys. Rev. C **104**, 054308 (2021).

DOI: 10.1103/PhysRevC.106.034321

I. INTRODUCTION

Proton elastic scattering is a useful tool for determining not only the neutron skin thickness of nuclei but also the detailed neutron density profile—in particular, the surface neutron density—as has been performed for various nuclei [1–6]. In recent years, experiments on 295 MeV (p, p) reactions [4–6] have been intensively performed to extract the neutron density by reaction analysis using the relativistic impulse approximation (RIA) with density-dependent effective NN interactions modified from the original Murdock and Horowitz model [7–9], called the ddMH model in this paper. The RIA+ddMH model [10] has successfully described the 295 MeV (p, p) reactions of various target nuclei, including Sn [4], Pb [5], and Ca [6] isotopes.

(p, p) cross sections are useful not only to determine the neutron radii, but also to extract information about the structure properties such as neutron single-particle properties and nuclear deformations, through their effects on the neutron density, which can be sensitively probed by the proton scattering. In a previous paper [11], 295 MeV Pb(p, p) reactions were analyzed, and it was demonstrated that the cross sections were sensitive to the single-particle occupation of the low-ℓ orbit in the major shell, which significantly contributes to the surface neutron density. A detailed analysis was performed focusing on the isotopic systematics of the nuclear structure properties and the reaction cross sections in a series of Pb isotopes. Isotopic analysis was demonstrated to be useful to reduce the systematic uncertainty in the data and the model ambiguities in the reaction analysis.

The present study aimed to extract the structure information on Sn isotopes from the experimental data of ^{A}Sn(p, p) cross sections at 295 MeV for $A = 116$–124 [4] by isotopic analysis combining structure and reaction calculations. The structure of the Sn isotopes was calculated using both relativistic Hartree-Bogoliubov (RHB) and nonrelativistic Skyrme Hartree-Fock-Bogoliubov (SHFB) calculations. Using the theoretical densities, the Sn(p, p) reactions were calculated with the RIA+ddMH model in the same way as in a previous study [11]. By comparing the calculated results and the experimental data, the isotopic systematics of the structure and reaction properties were investigated. Particular attention was paid to the change of the $3s_{1/2}$ neutron occupation from ^{116}Sn and ^{122}Sn, which can be sensitively probed by the isotopic systematics of the (p, p) cross sections through the effect on the surface neutron density.

This paper is organized as follows. The structure and reaction calculations are explained in Sec. II, and the calculated results are presented in Sec. III. In Sec. IV, the isotopic analysis is performed. Finally, a summary is provided in Sec. V.

II. CALCULATIONS OF NUCLEAR STRUCTURE AND PROTON ELASTIC SCATTERING

A. Structure calculations

The structure of even-even Sn isotopes with $A = 114$–124 was calculated by employing the spherical RHB and SHFB

calculations using the computational DIRHB code [12] and HFBRAD code [13], respectively. In the RHB calculations, the DD-ME2 [14] and DD-PC1 [15] interactions were used, which are denoted as me2 and pc1, respectively, in this paper. In the SHFB calculations, the SKM* [16] interaction with a mixed-type pairing force was used. SHFB calculations with the SLy4 [17] interaction were also performed; however, the resulting densities of the Sn isotopes were similar to those obtained using the SKM* interaction.

B. Calculations of proton elastic scattering reactions

The ^{A}Sn(p, p) reactions at $E_p = 295$ MeV were calculated using the RIA+ddMH model [10], in which real and imaginary nucleon-nucleus potentials were obtained by folding the target density with the effective NN interactions of the meson-exchange model. The RIA+ddMH model was constructed by introducing the density-dependent σ- and ω-meson masses and coupling constants for the effective NN interactions in the original Murdock and Horowitz model [7–9]. In the present calculation, the latest version of the parametrization of the RIA+ddMH model, which has been calibrated to fit the ^{58}Ni(p, p) data at 295 MeV [5], was employed.

The RIA+ddMH calculation was performed using the theoretical densities of the Sn isotopes obtained by the RMF and SHFB calculations. As structure inputs for calculating proton-nucleus potentials, the theoretical neutron $[\rho_n(r)]$ and proton $[\rho_p(r)]$ densities of the target nuclei were used for the neutron and proton vector densities, while $0.96\rho_n(r)$ and $0.96\rho_p(r)$ were used for the neutron and proton scalar densities, respectively, as performed in a previous study [11]. This prescription is the same as that performed in the analysis of the Sn(p, p) and Pb(p, p) reactions in Refs. [4,5].

III. RESULTS

A. Radii and densities of the Sn isotopes

The root-mean-square (rms) neutron (r_n) and proton (r_p) radii of the Sn isotopes using the RHB (me2 and pc1) and SHFB (SKM*) calculations are presented in Fig. 1(a), together with the experimental data. In all calculations, the theoretical r_p values reproduce the experimental data quite well. For r_n, the theoretical values are in reasonable agreement with the experimental data within the error bars except for ^{124}Sn.

The theoretical results of the neutron (ρ_n) and proton (ρ_p) densities of ^{116}Sn and ^{122}Sn are presented in Fig. 2, together with the experimental data from Ref. [4]. Comparing the me2, pc1, and SKM* results, all calculations obtain approximately consistent ρ_p and reproduce the experimental proton density reasonably well; however, the results for ρ_n depend somewhat on the structure models. As illustrated in Figs. 2(c) and 2(d), the peak position of $4\pi r^2\rho_n(r)$ shifts slightly to the right in the pc1 and SKM* results compared with the me2 results.

B. Sn(p, p) cross sections at 295 MeV

Figure 3 presents the Sn(p, p) cross sections at 295 MeV obtained from the RIA+ddMH calculations using the theoretical densities, together with the experimental data. The calculated cross sections at backward angles are sensitive to the detailed profile of the surface neutron densities. Compared with the experimental cross sections, the me2 density yields cross sections that are in reasonable agreement with the data, whereas the pc1 and SKM* densities do not. In the results calculated using the pc1 and SKM* densities, the diffraction pattern is shrunk, that is, the peak and dip positions at backward angles shift to forward angles and deviate significantly from the experimental data. This shrinkage of the diffraction pattern is caused by the outward shift of the surface-peak position of $4\pi r^2\rho(r)$ in the pc1 and SKM* densities, as illustrated previously in Figs. 2(c) and 2(d).

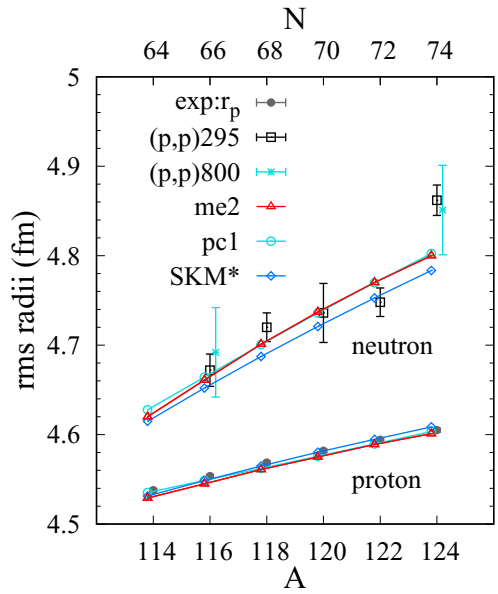

FIG. 1. rms neutron (r_n) and proton r_p radii of Sn isotopes. The theoretical values are the RHB (me2 and pc1) and the SHFB (SKM*) calculations. The experimental r_n values are those determined by the (p, p) reactions at both 295 MeV[4] and 800 MeV [2], while the experimental r_p values are obtained from the rms charge radii observed by isotope-shift measurements [18].

The me2 results are compared with the experimental cross sections in detail below. Calculation with the me2 density reproduces the ^{122}Sn(p, p) cross sections fairly well. For the ^{116}Sn(p, p) and ^{118}Sn(p, p) cross sections, calculation with the me2 density successfully reproduces the cross sections at forward angles; however, the agreement at backward angles is not satisfactory. Namely, the calculation somewhat overestimates the experimental cross sections. This overestimation at backward angles can be improved by a slight modification of the me2 densities for ^{116}Sn and ^{118}Sn.

For ^{120}Sn(p, p) and ^{124}Sn(p, p) cross sections, all calculations overestimate the peak amplitude of the data by 20–30% in the entire range of angles. In other words, the experimental cross sections for ^{120}Sn(p, p) and ^{124}Sn(p, p) seem unexpectedly small in the isotopic systematics. It is difficult to understand this global deviation from the experimental data because the peak amplitudes at forward angles $\theta_{\text{c.m.}} \approx 13^\circ$ are not sensitive to the detailed neutron density profile. The

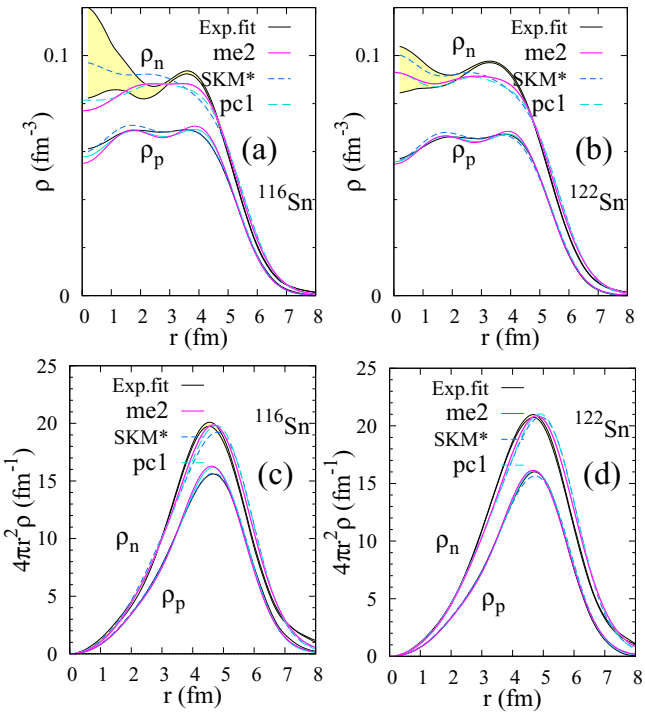

FIG. 2. Neutron (ρ_n^A) and proton (ρ_p^A) density distributions for ^{116}Sn and ^{122}Sn. (a) and (b) Neutron and proton density distributions for ^{116}Sn and ^{122}Sn, respectively, as obtained from the me2, pc1, and SKM* calculations. (c) and (d) The corresponding values of $4\pi r^2\rho$. The experimental neutron and proton densities from Ref. [4] are also presented ("Exp.fit"). The neutron density (error envelopes surrounded by thin lines) was determined by proton elastic scattering at 295 MeV, while the proton density (thin lines) was obtained from the charge distribution determined by electron elastic scattering.

normalization of the ^{120}Sn(p, p) and ^{124}Sn(p, p) data should be verified In the following analysis, I exclude the ^{120}Sn(p, p) and ^{124}Sn(p, p) data and mainly use the ^{116}Sn(p, p) and ^{122}Sn(p, p) data.

IV. ISOTOPIC ANALYSIS

Isotopic analysis using the systematics of the densities and cross sections in isotope chains is a powerful tool to extract structure information from the (p, p) data with less model uncertainty, as reported in a previous study [11]. For the isotopic analysis of ^{116}Sn(p, p) and ^{122}Sn(p, p), I define the isotopic cross section ratio of ^{122}Sn to ^{116}Sn as

$$R(\sigma;\theta_{\rm c.m.}) \equiv \frac{d\sigma(^{122}\mathrm{Sn})/d\Omega}{d\sigma(^{116}\mathrm{Sn})/d\Omega}, \quad (1)$$

where $d\sigma(^A\mathrm{Sn})/d\Omega$ is the differential cross sections for the ^{A}Sn(p, p) reactions in the center-of-mass frame. For the experimental values of $R(\sigma;\theta_{\rm c.m.})$, I omitted the mass difference in the transformation from the laboratory to center-of-mass frames.

The isotopic cross section ratio $R(\sigma)$ at 295 MeV calculated using the me2 and SKM* densities are displayed in Fig. 4, together with the experimental values. The ratio $R(\sigma)$

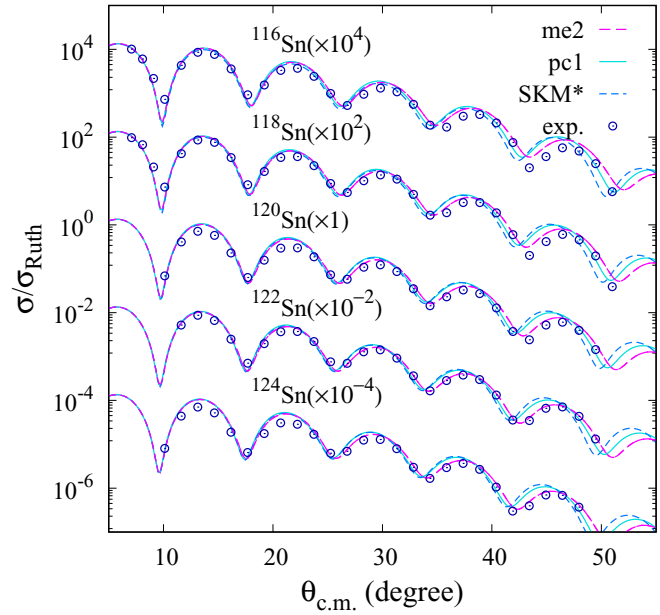

FIG. 3. Rutherford ratios of the Sn(p, p) cross sections at 295 MeV obtained from the RIA+ddMH calculations using the me2, pc1, and SKM* densities, together with the experimental data [4].

exhibits an oscillatory behavior that corresponds to the slight difference in the diffraction pattern of the cross sections between ^{116}Sn and ^{122}Sn, i.e., the diffraction pattern of ^{122}Sn slightly shrinks due to the increase in r_n compared with ^{116}Sn. In the isotopic analysis, the amplitude of the $R(\sigma)$ oscillation is important because it is sensitive to the detailed profile of the surface neutron density difference between ^{116}Sn and ^{122}Sn, whereas the interval of the oscillation of $R(\sigma)$ is less important. The results obtained using the me2 density underestimate the amplitude of the $R(\sigma)$ oscillation of the experimental data, particularly, at backward angles, whereas the calculation using the SKM* density well reproduces the peak magnitude of $R(\sigma)$, although the peak positions deviate somewhat from the data. The main origin of this difference in the peak magnitude between the two results is the single-particle occupation of the neutron $3s_{1/2}$ orbit, which significantly affects the surface

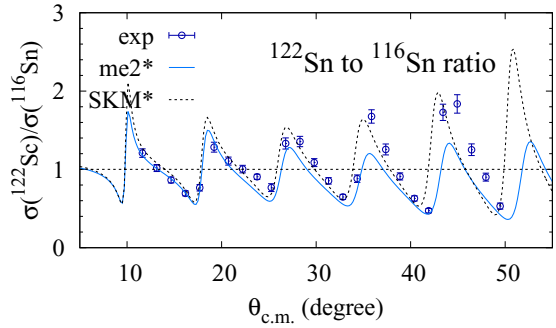

FIG. 4. Isotopic cross section ratio $R(\sigma)$ of ^{122}Sn(p, p) to ^{116}Sn(p, p) at 295 MeV. Theoretical results obtained by the RIA+ddMH calculations using the me2 and SKM* densities are compared with the experimental data [4].

TABLE I. Occupation probabilities of the $3s_{1/2}$, $2d_{3/2}$, and $1h_{11/2}$ orbits in ^{116}Sn and ^{122}Sn obtained from the me2 and SKM* calculations, together with the experimental data [19]. The isotopic difference in occupations between ^{122}Sn and ^{116}Sn is listed in boldface.

	ME2	SKM*	Expt.
		$3s_{1/2}$	
^{116}Sn	0.35	0.61	0.42(5)
^{122}Sn	0.80	0.80	0.56(5)
diff.	**0.46**	**0.20**	**0.14(7)**
		$2d_{3/2}$	
^{116}Sn	0.37	0.30	0.15(5)
^{122}Sn	0.80	0.60	0.39(5)
diff.	**0.43**	**0.30**	**0.24(7)**
		$1h_{11/2}$	
^{116}Sn	0.07	0.21	0.29(5)
^{122}Sn	0.30	0.43	0.54(5)
diff.	**0.23**	**0.22**	**0.25(7)**

neutron density. Table I lists the occupation probabilities of neutron $3s_{1/2}$, $2d_{3/2}$, and $1h_{11/2}$ in ^{122}Sn and ^{116}Sn obtained by the me2 and SKM* calculations, in comparison with the experimental data determined by neutron transfer and pickup experiments [19]. For each orbit, the isotopic difference of the occupations between ^{122}Sn and ^{116}Sn is also listed. The isotopic difference of the $3s_{1/2}$ occupation is as large as 0.46 in the me2 results, which is three times larger than the experimental value of 0.15, whereas in the SKM* results it is in reasonable agreement with the experimental value. In other words, the me2 calculation yields a rapid increase of the $3s_{1/2}$ occupation from ^{116}Sn to ^{122}Sn, which is inconsistent with the modest change of the occupation in the experimental data and the SKM results.

The neutron single-particle energies obtained by the me2 and SKM* calculations are presented in Fig. 5, together with the experimental data, while the occupation probability of neutron single-particle orbits in Sn isotopes is presented in Fig. 6. In the me2 results, the $3s_{1/2}$ and $2d_{3/2}$ are almost degenerate, and they have an approximately 2 MeV energy gap from the lower orbits ($2d_{5/2}$ and $1g_{7/2}$) (see Fig. 5). As a result, the $3s_{1/2}$ and $2d_{3/2}$ occupation rapidly increases with an increase in N in the me2 case [Fig. 6(a)]. In contrast, the SKM* calculation obtains a lower $3s_{1/2}$ orbit than the $2d_{3/2}$ orbit. In this case, the $3s_{1/2}$ orbit is already half occupied in ^{114}Sn, and the $3s_{1/2}$ occupation gradually changes with the increase in N [Fig. 6(b)]. This $3s_{1/2}$-$2d_{3/2}$ level spacing in the SKM* calculation is consistent with that of the experimental single-particle energies and yields a modest N dependence of the $3s_{1/2}$ occupation, in contrast to the me2 results.

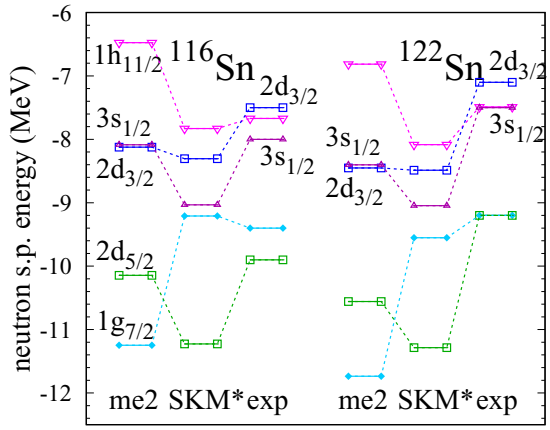

FIG. 5. Neutron single-particle energies in ^{116}Sn and ^{122}Sn obtained from the me2 and SKM* calculations compared with the experimental data from Ref. [19].

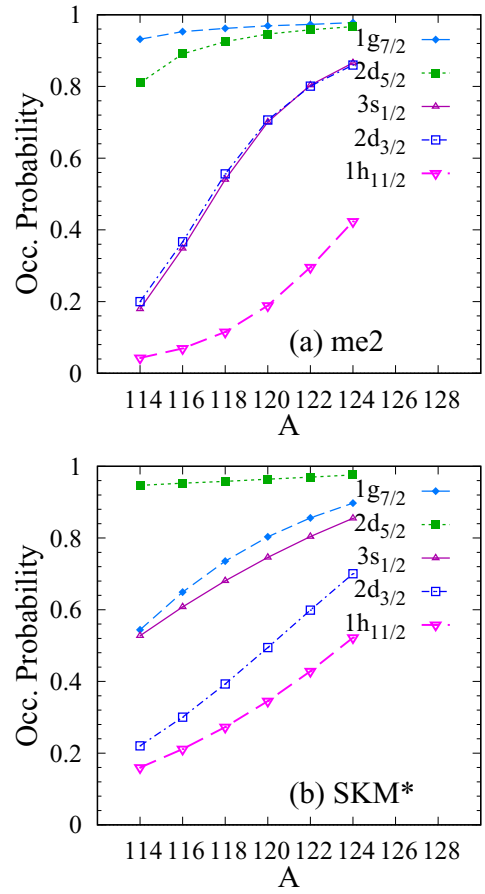

FIG. 6. Occupation probabilities of neutron single-particle orbits in the Sn isotopes obtained from the (a) me2 and (b) SKM* calculations.

The failure in reproducing the peak magnitude of $R(\sigma)$ of the (p, p) reaction, presented in Fig. 4, is caused by the rapid increase of the $3s_{1/2}$ occupation from ^{116}Sn to ^{122}Sn in the me2 calculation through its contribution to the surface neutron density. To demonstrate the sensitivity of $R(\sigma)$ to the change of the $3s_{1/2}$ occupation, I performed a model analysis by changing the $3s_{1/2}$ occupation in ^{116}Sn from the original me2 result by hand. The model density of ^{116}Sn is given as

$$\rho^{116}_{n,\mathrm{model}}(r) = \left(1 - \frac{1}{N}\right)\rho^{116}_{n}(r) + \rho^{\mathrm{s.p.}}_{3s_{1/2}}(r), \qquad (2)$$

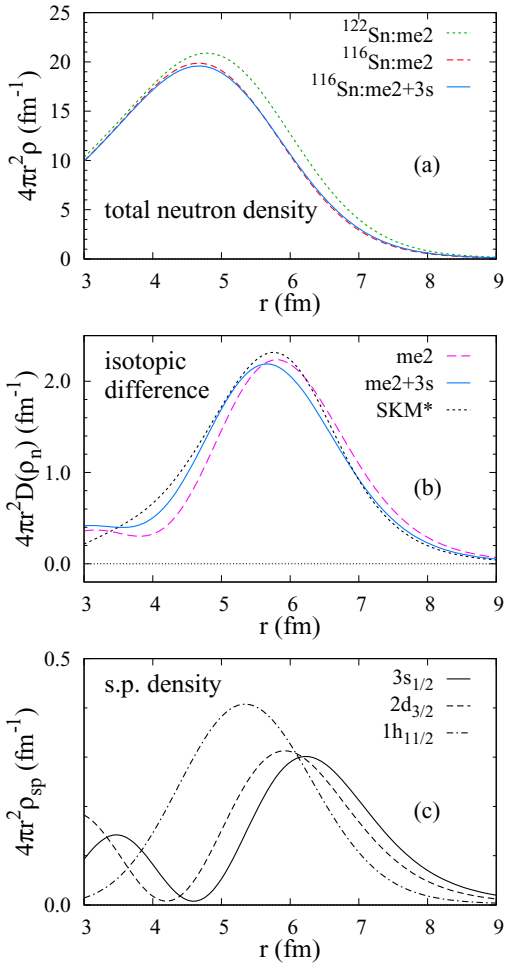

FIG. 7. (a) Neutron densities of ^{116}Sn for the me2 and me2+3s densities. For reference, the neutron density of ^{122}Sn is also presented. (b) Isotopic difference in the neutron density of ^{122}Sn from ^{116}Sn obtained for the me2, me2+3s, and SKM* densities. (c) Single-particle densities $\rho^{\text{s.p.}}(r)$ of the $3s_{1/2}$, $2d_{3/2}$, and $1h_{11/2}$ orbits in ^{120}Sn obtained from the me2 calculation.

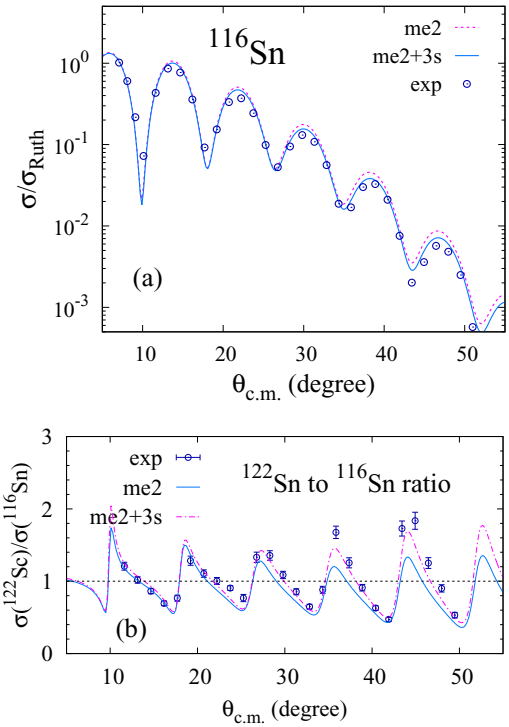

FIG. 8. (a) The ^{116}Sn(p, p) cross sections at 295 MeV and (b) isotopic cross section ratios $R(\sigma)$ of ^{122}Sn(p, p) to ^{116}Sn(p, p) obtained by the RIA+ddMH calculations using the me2 and me2+3s densities, compared with the experimental data [4].

where $\rho^{\text{s.p.}}_{3s_{1/2}}(r)$ is the single-particle density of the neutron $3s_{1/2}$ orbit. In this model (called the "me2+3s model") the density in ^{122}Sn was unchanged, while the $3s_{1/2}$ occupation number in ^{116}Sn was increased by 1 from the original me2 density, corresponding to the increase of the $3s_{1/2}$ occupation probability by 0.5. After the increase, the $3s_{1/2}$ occupation in ^{116}Sn became almost the same as that in ^{122}Sn. Figure 7(a) compares the me2 and me2+3s neutron densities of ^{116}Sn, together with those in ^{120}Sn, while Fig. 7(c) represents the neutron single-particle densities of $3s_{1/2}$, $2d_{3/2}$, and $1h_{11/2}$ obtained by the me2 calculation for ^{120}Sn.

Due to the modification of the $3s_{1/2}$ occupation in ^{116}Sn, the surface neutron density around $r = 4$–5 fm decreases from the original me2 density [see blue solid and magenta dashed lines at the peak of $4\pi r^2$ in Fig. 7(a)]. To examine the isotopic change of the neutron density more closely, I defined the isotopic neutron density difference between ^{116}Sn and ^{122}Sn as

$$D(\rho_n; r) \equiv \rho_n(^{122}\text{Sn}; r) - \rho_n(^{116}\text{Sn}; r). \tag{3}$$

Figure 7(b) represents the values of $4\pi r^2 D(\rho_n; r)$ obtained for the me2, me2+3s, and SKM* densities. $D(\rho_n; r)$ of the me2 density is dominantly contributed by the major-shell orbits, $3s_{1/2}$, $2d_{3/2}$, and $1h_{11/2}$. $D(\rho_n; r)$ around $r = 4$–5 fm is significantly larger in the me2+3s and SKM* densities than the me2 density due to the modest change of the $3s_{1/2}$ occupation from ^{116}Sn to ^{122}Sn. In contrast, $D(\rho_n; r)$ at the nuclear surface is smaller because the rapid increase of the $3s_{1/2}$ occupation reduce the $D(\rho_n; r)$ in the $r = 4$–5 fm region.

Using the modified ^{116}Sn density of me2+3s, I calculated the ^{116}Sn(p, p) cross sections and the isotopic cross section ratio $R(\sigma)$. Figure 8 compares the results obtained by employing the me2+3s and me2 densities. As expected, the me2+3s density yields an improved result of the ^{116}Sn(p, p) cross sections at backward angles [Fig. 7(a)]. Moreover, the result of $R(\sigma)$ is significantly improved in the me2+3s calculation and agrees well with the experimental data [Fig. 7(b)].

In general, $R(\sigma)$ of 295 MeV (p, p) reactions is a sensitive probe of the occupation change of low-ℓ orbits, as discussed in previous work [11]. I performed a similar analysis by changing the neutron occupation numbers of $2d_{3/2}$ and $1h_{11/2}$ in ^{116}Sn and verified that the peak amplitudes of $R(\sigma)$ were not as sensitive to the $2d_{3/2}$ and $1h_{11/2}$ occupations as to the $3s_{1/2}$ occupation. It should be emphasized again that the peak amplitude of $R(\sigma)$ of ^{122}Sn to ^{116}Sn at backward angles is

sensitive to the isotopic neutron density difference $D(\rho_n; r)$ at the nuclear surface around $r = 4$–5 fm and is affected by the isotopic change of the $3s_{1/2}$ occupation. The conclusion derived from the present analysis is that a rapid increase of the $3s_{1/2}$ occupation from ^{116}Sn to ^{122}Sn obtained in the me2 calculation is unlikely.

V. SUMMARY

The isotopic analysis of Sn isotopes in the range $A = 116$–124 was performed by combining the nuclear structure and reaction calculations. ^{A}Sn(p, p) reactions at 295 MeV were calculated using the RIA+ddMH model with theoretical densities for the Sn isotopes obtained from RHB and SHFB calculations. The RIA+ddMH calculations using the theoretical density from the RHB calculations with the me2 interaction (i.e., DD-ME2 interaction) were in reasonable agreement with the experimental cross sections; however, they somewhat overestimated the backward cross sections of the ^{116}Sn(p, p) and ^{118}Sn(p, p) reactions.

A detailed analysis of the isotopic systematics was performed by using the isotopic cross section ratios $R(\sigma)$ of ^{122}Sn to ^{116}Sn. Comparing the theoretical $R(\sigma)$ with the experimental values, the peak amplitudes of $R(\sigma)$ at backward angles were significantly underestimated by the me2 density, whereas they were well reproduced by the SKM* density. The main cause of the underestimation of the me2 result was found to be the $3s_{1/2}$ neutron contribution. The $3s_{1/2}$ occupation probability rapidly increased with an increase in N in the me2 calculation; however, this was inconsistent with the experimental observation of only a small increase from ^{116}Sn to ^{122}Sn.

To demonstrate the sensitivity of $R(\sigma)$ to the $3s_{1/2}$ neutron contribution, model analysis (me2+3s) was performed by modifying the neutron $3s_{1/2}$ occupation in ^{116}Sn. It was proved that the ^{116}Sn(p, p) cross sections at backward angles were sensitive to the $3s_{1/2}$ neutron contribution. This signifies that the peak amplitudes of $R(\sigma)$ of ^{122}Sn to ^{116}Sn serve as a sensitive probe of the isotopic change of the neutron $3s_{1/2}$ occupation through its effect on the isotopic difference $D(\rho_n; r)$ of the surface neutron density in the $r = 4$–5 fm region. In the model calculation using the me2+3s density, the peak amplitudes of $R(\sigma)$ at backward angles were reproduced well. The good reproduction of the experimental $R(\sigma)$ indicates that a rapid increase of the $3s_{1/2}$ occupation from ^{116}Sn to ^{122}Sn obtained by the me2 calculation is unlikely. This result derived from the 295 MeV ^{A}Sn(p, p) cross section data [4] is consistent with the direct measurement of neutron occupations in Sn isotopes by the neutron transfer and pickup reactions [19].

ACKNOWLEDGMENTS

This work was supported by Grants-in-Aid of the Japan Society for the Promotion of Science (Grants No. JP18K03617, No. JP18H05407, and No. JP22K03633) and by a grant of the joint research project of the Research Center for Nuclear Physics at Osaka University.

[1] L. Ray, W. R. Coker, and G. W. Hoffmann, Uncertainties in neutron densities determined from analysis of 0.8-GeV polarized proton scattering from nuclei, Phys. Rev. C **18**, 2641 (1978).

[2] L. Ray, Neutron isotopic density differences deduced from 0.8 GeV polarized proton elastic scattering, Phys. Rev. C **19**, 1855 (1979); **20**, 1212(E) (1979).

[3] G. W. Hoffmann, L. Ray, M. Barlett, J. McGill, G. S. Adams, G. J. Igo, F. Irom, A. T. M. Wang, C. A. Whitten, R. L. Boudrie, J. F. Amann, C. Glashausser, N. M. Hintz, G. S. Kyle, and G. S. Blanpied, 0.8 GeV p+^{208}Pb elastic scattering and the quantity $\Delta r_{\rm np}$, Phys. Rev. C **21**, 1488 (1980).

[4] S. Terashima, H. Sakaguchi, H. Takeda, T. Ishikawa, M. Itoh, T. Kawabata, T. Murakami, M. Uchida, Y. Yasuda, M. Yosoi, J. Zenihiro, H. P. Yoshida, T. Noro, T. Ishida, S. Asaji, and T. Yonemura, Proton elastic scattering from tin isotopes at 295 MeV and systematic change of neutron density distributions, Phys. Rev. C **77**, 024317 (2008).

[5] J. Zenihiro, H. Sakaguchi, T. Murakami, M. Yosoi, Y. Yasuda, S. Terashima, Y. Iwao, H. Takeda, M. Itoh, H. P. Yoshida, and M. Uchida, Neutron density distributions of ^{204,206,208}Pb deduced via proton elastic scattering at $E_p = 295$ MeV, Phys. Rev. C **82**, 044611 (2010).

[6] J. Zenihiro *et al.*, Direct determination of the neutron skin thicknesses in ^{40,48}Ca from proton elastic scattering at $E_p = 295$ MeV, arXiv:1810.11796.

[7] C. J. Horowitz, Relativistic Love-Franey model: Covariant representation of the NN interaction for N-nucleus scattering, Phys. Rev. C **31**, 1340 (1985).

[8] D. P. Murdock and C. J. Horowitz, Microscopic relativistic description of proton-nucleus scattering, Phys. Rev. C **35**, 1442 (1987).

[9] C. J. Horowitz, D. P. Murdock, and B. D. Serot, in *Computational Nuclear Physics 1*, edited by K. Langanke, J. Maruhn, and S. Koonin (Springer-Verlag, Berlin, 1991), p. 129.

[10] H. Sakaguchi *et al.*, Elastic scattering of polarized protons from ^{58}Ni at $E_p = 192$, 295, and 400 MeV, Phys. Rev. C **57**, 1749 (1998).

[11] Y. Kanada-En'yo, Isotopic analysis of 295 MeV proton scattering off ^{204,206,208}Pb for improvement of neutron densities and radii, arXiv:2106.00151.

[12] T. Nikšić, N. Paar, D. Vretenar, and P. Ring, DIRHB - A relativistic self-consistent mean-field framework for atomic nuclei, Comput. Phys. Commun. **185**, 1808 (2014).

[13] K. Bennaceur and J. Dobaczewski, Coordinate-space solution of the Skyrme-Hartree-Fock-Bogolyubov equations within spherical symmetry. The program HFBRAD (v1.00), Comput. Phys. Commun. **168**, 96 (2005).

[14] G. A. Lalazissis, T. Nikšić, D. Vretenar, and P. Ring, New relativistic mean-field interaction with density-dependent meson-nucleon couplings, Phys. Rev. C **71**, 024312 (2005).

[15] T. Nikšić, D. Vretenar, and P. Ring, Relativistic nuclear energy density functionals: Adjusting parameters to binding energies, Phys. Rev. C **78**, 034318 (2008).

[16] J. Bartel, P. Quentin, M. Brack, C. Guet, and H. B. Hakansson, Towards a better parametrisation of Skyrme-like effective

forces: A Critical study of the SkM force, Nucl. Phys. A **386**, 79 (1982).

[17] E. Chabanat, P. Bonche, P. Haensel, J. Meyer, and R. Schaeffer, A Skyrme parametrization from subnuclear to neutron star densities. 2. Nuclei far from stablities, Nucl. Phys. A **635**, 231 (1998); **643**, 441(E) (1998).

[18] I. Angeli and K. P. Marinova, Table of experimental nuclear ground state charge radii: An update, At. Data Nucl. Data Tables **99**, 69 (2013).

[19] S. V. Szwec *et al.*, Neutron occupancies and single-particle energies across the stable tin isotopes, Phys. Rev. C **104**, 054308 (2021).